Supporting Information For

Multifunctional Conductive Hydrogels with Low Hysteresis, Excellent Water Retention and Anti-Freezing as Flexible Wearable Sensors

Binhang Yuan,[a] Ying Yue,[a] Qinxue Wang,[a] Huijing Han,[a] Meiran Xie,[a] and Xiaojuan Liao*[a]

[a] *School of Chemistry and Molecular Engineering, East China Normal University, Shanghai 200062, P. R. China*

* Corresponding author.

E-*mail address:* xjliao@chem.ecnu.edu.cn (X. Liao)

Table of Contents:

1. Materials and methods

Di (ethylene glycol) methyl ether acrylate (EGA), AM, LiCl, *N, N'*-methylenebis (acrylamide) (MBAA), *N, N, N′, N′*-tetramethylethylenediamine (TEMED) and ammonium persulfate (APS) were purchased from Adamas-beta. Capacitive carbon electrode were purchased from Shanghai Yanwen Technology Co., Ltd. All the chemicals were used as purchased without further purification.

Fourier transform infrared spectroscopy is an important spectroscopic technique used to analyze the functional groups, molecular structure, and bonding modes of materials. In this study, a Nicolet IS50 FT-IR spectrometer was used to test solid samples in attenuated total reflection mode (ATR-FTIR) with air as the background, covering a wavelength range of 4000 - 500 cm^{-1}.

Differential scanning calorimetry (DSC) is a thermal analysis technique primarily used to characterize the thermal effects generated by materials during programmed temperature increase or decrease. This study utilized a DSC3500 differential scanning calorimeter for testing. A 5-10 mg hydrogel sample was sealed in an aluminum crucible, with nitrogen serving as both the protective and purge gas at a flow rate of 50 $mL \cdot min^{-1}$. The heating rate was set at 5 $^{o}C \cdot min^{-1}$, and the testing temperature range spanned from -90 to 20 ^{o}C.

Raman spectroscopy is an important characterization method used to study the molecular vibrational modes, chemical structure, and bonding state of materials. In this study, an argon ion laser with a wavelength of 633 nm was employed as the excitation light source for direct characterization of the samples.

X-ray photoelectron spectroscopy (XPS) was employed to analyze the elemental composition, chemical environment, chemical bonding, and other information of solid electrolytes. An Al-Ka laser is used as the emission source (hv=1486.8 eV), with a beam spot size of 400mm, and the standard baseline is set using C 1s (284.8 eV) as the standard.

The electrochemical impedance spectroscopy (EIS) analysis of the conductive hydrogels was performed in a frequency range of $10^{-2} \times 10^{5}$ Hz using

a CHI660E electrochemical workstation (Chenhua Co., China). The size of the conductive hydrogel used for EIS detection was 15 × 9 × 4.5 mm. The ionic conductivity (σ) was calculated using the following equation.

$$\sigma = \frac{L}{R \times A} \#\ (1)$$

where L is the thickness of the hydrogel sample (m); R is the body impedance of the measured sample (ohm), which was obtained from the intersection of the semi-arc and oblique lines in the Nyquist plot of the EIS spectrum; A is the effective cross-section area between the electrodes and hydrogel (m^2).

The mechanical properties of hydrogels were measured by an electronic universal testing machine (HY-0508, Shanghai Hengyi) at room temperature. The tensile speed is 50 mm/min, using a 50 N sensor. The rectangular specimens used for sample preparation measured approximately 6.6 mm × 15.0 mm × 3.0 mm. Regarding the load-unload cycle test, the tensile speed is 25 mm/min.

The rheological properties of the hydrogel samples, specifically the storage modulus (G') and loss modulus (G''), were measured as a function of angular frequency using an MCR302 rheometer manufactured by Anton Paar, Austria. A 25 mm cone rotor was employed, and the temperature was maintained at 25 °C throughout the testing process. The rheological test in this study was conducted with a shear strain of 0.5% and an angular frequency ranging from 0.1 to 100 rad/s.

Different hydrogel samples were placed at different ambient environments. The water retention ability of hydrogels at different time was calculated by the following equation:

$$Water\ retention\ (\%) = \frac{m_x}{m_0} \times 100\% \#\ (2)$$

Where m_0 and m_x were the weight of hydrogels at the beginning and after x hours, respectively.

PAM-PEGA-Li-2 hydrogels were dehydrated at 60 °C in vacuo for 4 h. Afterward, the dehydrated hydrogels were placed at 25 °C and 80% RH environments for different time. The self-regeneration ability of hydrogels was determined by the following equation:

$$Water\ ratio\ (\%) = \frac{m_d}{m_0} \times 100\%\#\ (3)$$

Where m_0 was the initial weight of undehydrated hydrogels, and m_d was the weight of dehydrated hydrogels after a self-regeneration period of one day.

The electrochemical performance of the flexible all-solid-state supercapacitors was evaluated using cyclic voltammetry (CV) and galvanostatic charge-discharge (GCD) curves. All electrochemical characterization methods were conducted on a electrochemical workstation (CHI660E). The specific capacitance of the supercapacitors was calculated according to the following equation:

$$C_s = \frac{I \times \Delta t}{S \times \Delta E}\#\ (4)$$

Where I (mA) is the discharge current, $\Delta t\ (s)$ is the discharge time, S (cm^2) is the total area of the active substance, and $\Delta E\ (V)$ is the voltage of the discharge drop.

2. Preparation of the hydrogels

Hydrogels with different feeding ratios were prepared (Table 1). As an example, sample PAM-PEGA-Li-2 was prepared as follows. 0.09 g of EGA (0.48 mmol) and 0.59 g of AM (8.30 mmol) were dissolved in 2 mL of deionized water. After thorough mixing, 0.5 g of LiCl (11.80 mmol), 0.2 mg cross-linker MBAA (0.15% of the monomeric molar amount), 10 uL of catalyst (TEMED, 0.06 mmol) and 10 mg of initiator (APS, 0.04 mmol) were added to the above solution. The well-mixed prepolymerization solution was injected into a mold and heated in an oven at 60 °C for 1 h to obtain the conductive hydrogel.

3. High-resolution O 1s XPS spectra

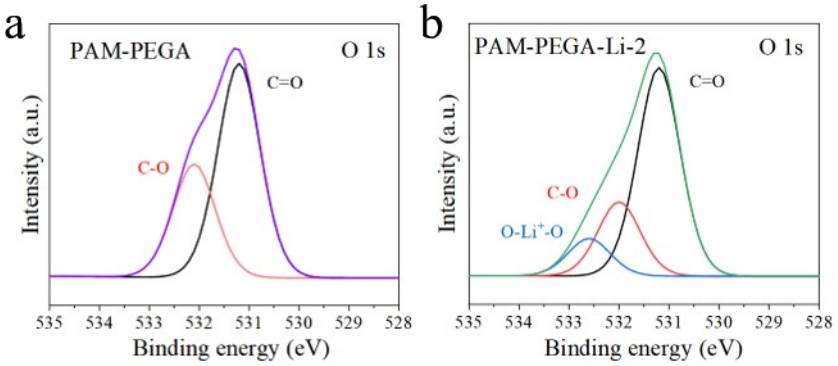

Figure S1. Deconvoluted O 1s spectra of PAM-PEGA (a) and PAM-PEGA-Li-2 (b).

Compared with PAM-PEGA, a new component appears in the O 1s spectrum of PAM-PEGA-Li-2 at lower binding energy, which can be attributed to Li^+-O coordination. The C-O peak also exhibits slight changes and peak broadening, indicating modification of the oxygen chemical environment. These results confirm the formation of Li-O coordination interactions within the hydrogel network.[1-3]

4. Mechanical properties of the different hydrogels

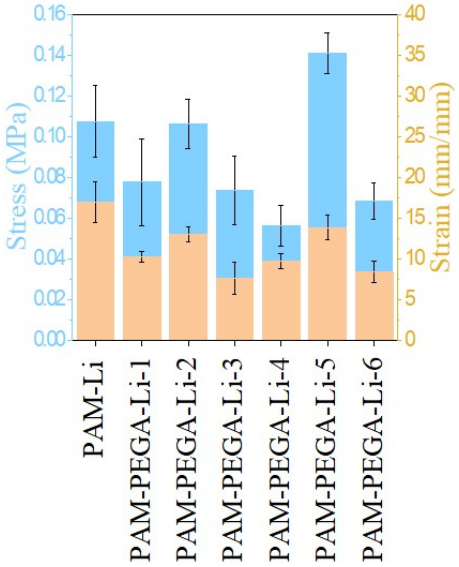

Figure S2. Stress-strain of different hydrogel samples at a strain rate of 50 mm/min.

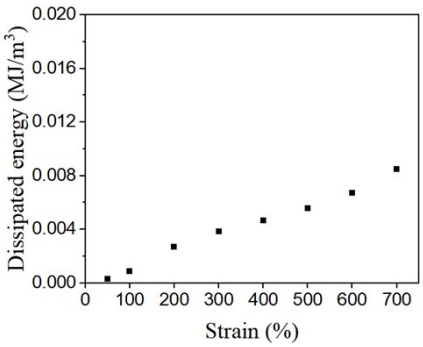

Figure S3. The dissipated energy of the loading-unloading tensile curves of PAM-EGA-Li-2 hydrogel within the strain range of 50% to 700%.

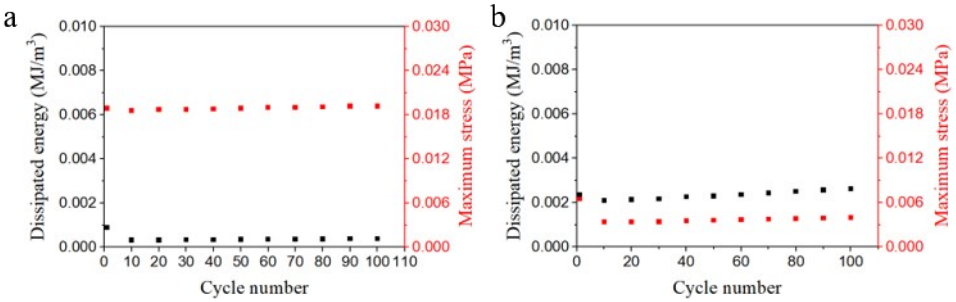

Figure S4. Tensile loading-unloading cycles of the hydrogel under 100% strain at a deformation rate of 25 mm/min for 100 cycles. Dissipated energy and maximum stress of the PAM-PEGA-Li-2 hydrogel (a) and PAM-Li hydrogel (b).

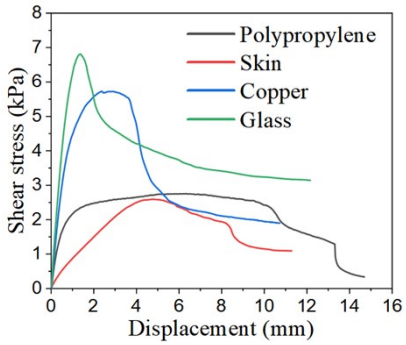

Figure S5. Adhesion performance of PAM-PEGA-Li-2 hydrogels.

Figure S5 presents the adhesion performance of PAM-PEGA-Li-2 hydrogels on different substrates, including polypropylene, skin, copper, and glass. The shear stress-displacement curves show that the hydrogel exhibits substrate-dependent adhesion behavior. Among the tested surfaces, the hydrogel displays relatively higher shear strength on copper (~7 kPa) and glass (~6 kPa), which can be attributed to the presence of polar groups on these surfaces that promote hydrogen bonding

and dipole-dipole interactions with the hydrophilic functional groups in the hydrogel. In contrast, adhesion to polypropylene and skin is weaker due to their low surface energy and limited hydrogen-bonding capability. Overall, these results indicate that the adhesion of PAM-PEGA-Li-2 hydrogels varies with substrate polarity and surface energy, suggesting moderate interfacial interactions rather than strong adhesion.

5. Low-temperature mechanical properties

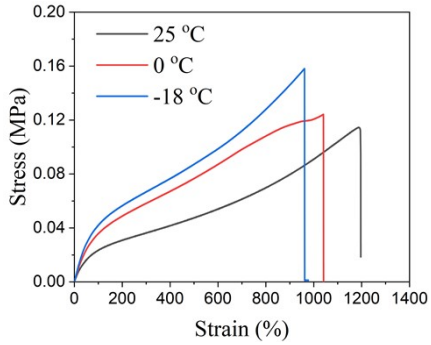

Figure S6. Low-temperature mechanical properties of PAM-PEGA-Li-2 hydrogel

As shown in Figure S6, the hydrogel maintains good stretchability at -18 °C and 0 °C, exhibiting comparable stress-strain behavior to that at 25 °C. Although slight variations in tensile strength and elongation are observed, the hydrogel remains highly deformable without brittle fracture, demonstrating its excellent low-temperature mechanical stability.

6. DSC curves of the different hydrogels

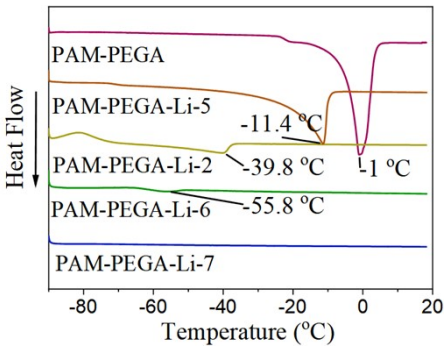

Figure S7. DSC heating curves of hydrogels with different LiCl contents

7. The effect of EGA on the moisturizing and antifreeze properties of samples

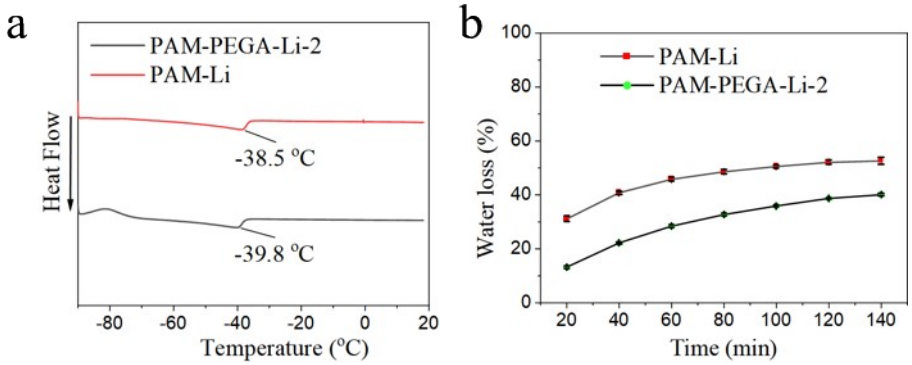

Figure S8. (a) DSC curves of PAM-Li and PAM-PEGA-Li-2 hydrogels; (b) Water loss rate of the two hydrogels at 80 °C**.**

8. Photos of the PAM-PEGA hydrogel as part of the circuit.

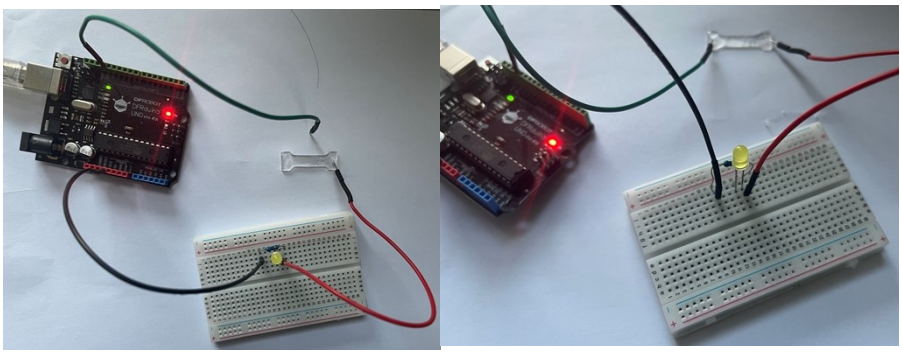

Figure S9. Photos of the PAM-PEGA hydrogel as part of the circuit when the circuit was open (left) and closed (right).

9. Photos of the super capacitor.

Figure S10. Front (left) and side (right) views of the super capacitor.

10. The performance of different hydrogel electrolytes.

Table S1. The mechanical properties, conductivities, and freezing points of different hydrogel electrolytes.

Electrolyte	Stretchability (%)	Maximum stress (MPa)	Conductivity (S/m)	Freezing temperature (°C)	Ref.
P(AM-*co*-EGA)/LiCl	**1297**	**0.106**	**10.28**	**-39.8**	**This work**
P(SBMA-*co*-HEA)/ LiCl	270	0.052	1.26	-40	4
PAM/CNF/LiCl	750	0.08	9.97	< -80	5
Glu/P(HEA-*co*-AA)-Fe/LiCl	1213	4.15	0.43	< -60	6
Gelatin/ PAA-NHS ester/Gly	850	0.28	0.9	-29.5	7
EDH/PVA/LiCl	45	0.28	3	N/A	8
P(SBMA-*co*-AA)/LiCl	420	0.025	11	< -80	9

P(AM-*co*-SBMA)/PVA/LiCl	1350	0.13	7.95	-45.3	10
PAM/WSCA/LiCl	1580	0.135	16.7	< -80	11
P(AM-*co*-AEAM-MTAC)/MWCNT/LiCl	4075	1.09	0.85	N/A	12
PAM/CMC/LiCl	102	0.88	5.21	< -80	13
P(AM-*co*-AEAM)/ F127CHO/MWCNT/ LiCl	1200	0.15	3.96	N/A	14
Cellulose/BT/LiCl	98	0.78	8.99	-28.9	15
PAM/LiCl	480	0.03	4.47	< -70	16
PSBMA/Clay/LiCl	1300	0.045	1.71	< -60	17
PVA/PEI/LiCl	7000	0.01	0.12	-80	18
PVA/LiCl	1750	1.7	5.61	-52.4	19
PNIAM/GO/LiCl	1821	2.18	4.3	-54	20

11. The performance of different supercapacitors.

Table S2. The performance of different supercapacitors.

Electrolyte	Active material	specific capacitance	cycling performance (RT. or 25 °C)	Coulombic efficiency	Ref.
P(Am-*co*-EGA)/ LiCl	**AC**	**124.3 mF/cm^2 (0.5 mA/cm^2)**	**10000/101.9%**	**100%**	**This work**
PAM-DVB-Li	PANI	469 mF/cm^2 (0.5 mA/cm^2)	6000/89%	96.1%	21
PAA/DES/CNF	Porous carbon	94.4 F/g (1 A/g)	5000/90.1%	N/A	22
ASPL/AA/Am/SA	AC	69.4 mF/cm^2 (0.5 A/g)	10000/115%	≈100%	23
PVA/PI/LiCl/ DMSO/H_2O	AC	139.9 mF/cm^2 (1.67 mA/cm^2)	10000/95.3%	N/A	24
P(NAGA-*co*-VTZ)/KCl	acNTs	282.62 F/g (0.2 A/g)	10000/97%	N/A	25
PVA/LiCl/$CaCl_2$	MXene/BC and PANI/CNT	372.1 mF/cm^2 (0.5 mA/cm^2)	5000/88.9%	99%	26

SNFs/PGP/$ZnSO_4$/H_2O/EG	AC	0.5A/g (82.14 F/g)	40000/98.2%	100%	27
PEDOT:PSS/ C-MXene/ GA-PVA	PVA-H_3PO_4 gel electrolyte	303.6 mF/cm^2 (1 mA/cm^2)	1000/81%	N/A	28
PSBMA/CMC/ MXene/$ZnCl_2$	AC/CC cathodes with Zn anodes	247 F/g (1 A/g)	5000/97.5%	100%	29

References

1. T. Liu, Y. Zhong, Z. Yan, B. He, T. Liu, Z. Ling, B. Li, X. Liu, J. Zhu, L. Jiang, X. Gao, R. Zhang, J. Zhang, B. Xu and G. Zhang, *Angew. Chem. Int. Ed.*, 2024, **63**, e202411535.
2. E. B. Springl, D. Sarkar, M. Mühlau, V. K. Michaelis and T. Nilges, *Inorg. Chem.*, 2025, **64**, 19752-19763.
3. D. Martin-Vosshage and B. V. R. Chowdari, *Electrochim. Acta*, 1995, **40**, 2109-2114.
4. J. Yang, Z. Xu, J. Wang, L. Gai, X. Ji, H. Jiang and L. Liu, *Adv. Funct. Mater.*, 2021, **31**, 2009438.
5. W. Ge, S. Cao, Y. Yang, O. J. Rojas and X. Wang, *Chem. Eng. J.*, 2021, **408**, 127306.
6. H. Zhang, Q. Yang, L. Xu, N. Li, H. Tan, J. Du, M. Yu and J. Xu, *Nano Energy*, 2024, **125**, 109521.
7. Y. Niu, H. Liu, R. He, M. Luo, M. Shu and F. Xu, *Small*, 2021, **17**, 2101151.
8. L. Xu, Y. Pan, X. Wang, Z. Xu, H. Tian, Y. Liu, X. Bu, H. Jing, T. Wang, Y. Liu and M. Liu, *ACS Appl. Mater. Interfaces*, 2023, **15**, 4458-4468.
9. X. Sui, H. Guo, C. Cai, Q. Li, C. Wen, X. Zhang, X. Wang, J. Yang and L. Zhang, *Chem. Eng. J.*, 2021, **419**, 129478.
10. Y. Wang, P. Chen, X. Zhou, Y. Liu, N. Wang and C. Gao, *ACS Appl. Mater. Interfaces*, 2022, **14**, 47100-47112.
11. K. Zhang, Y. Pang, C. Chen, M. Wu, Y. Liu, S. Yu, L. Li, Z. Ji and J. Pang, *Carbohydr. Polym.*, 2022, **293**, 119673.
12. M. Wu, M. Pan, C. Qiao, Y. Ma, B. Yan, W. Yang, Q. Peng, L. Han and H. Zeng, *Chem. Eng. J.*, 2022, **450**, 138212.
13. Y. Lu, Y. Yue, Q. Ding, C. Mei, X. Xu, S. Jiang, S. He, Q. Wu, H. Xiao and J. Han, *InfoMat*, 2023, **5**, e12409.
14. M. Wu, J. Chen, Y. Ma, B. Yan, M. Pan, Q. Peng, W. Wang, L. Han, J. Liu and H. Zeng, *J. Mater. Chem. A*, 2020, **8**, 24718-24733.
15. J. Manigrasso, I. Chillón, V. Genna, P. Vidossich, S. Somarowthu, A. M. Pyle, M. De Vivo and M. Marcia, *Nat. Commun.*, 2022, **13**, 1.
16. J. Chen, C. Shi, L. Wu, Y. Deng, Y. Wang, L. Zhang, Q. Zhang, F. Peng, X.-M. Tao, M. Zhang and W. Zeng, *ACS Appl. Mater. Interfaces*, 2022, **14**, 34714-34721.
17. Y. Chen, C. Zhang, R. Yin, A. Yin, Q. Feng, F. Liu, J. Shao, T. Su, H. Wang, G. Chen and W. Zhao, *Chem. Eng. J.*, 2022, **449**, 137907.
18. C. Wang, Y. Liu, X. Qu, B. Shi, Q. Zheng, X. Lin, S. Chao, C. Wang, J. Zhou, Y. Sun, G. Mao and Z. Li, *Adv. Mater.*, 2022, **34**, 2105416.
19. C. Tang, Y. Yao, M. Li, Y. Wang, Y. Zhang, J. Zhu, L. Wang and L. Li, *Adv. Funct. Mater.*, 2025, **35**, 2417207.
20. Y. Yang, C. Yao, W.-Y. Huang, C.-L. Liu and Y. Zhang, *ACS Appl. Mater. Interfaces*, 2024, **16**, 11957-11972.
21. Y. Li, X. Wei, F. Jiang, Y. Wang, M. Xie, J. Peng, C. Yi, J. Li and M. Zhai, *Energy Environ. Mater.*, 2025, **8**, e12820.
22. L.-H. Xu, Y.-T. He, Y. Xu, S. Sun, J. Liu, J. Yang, J.-L. Wen and T.-Q. Yuan, *Adv. Funct. Mater.*, 2025, **35**, 2501263.
23. J. Luo, L. Lyu, Z. Yin and Y. Wei, *Front. Chem. Sci. Eng.*, 2024, **19**, 4.
24. Q. Zhou, A. Griffin, J. Qian, Z. Qiang, B. Sun, C. Ye and M. Zhu, *Adv. Funct. Mater.*, 2024, **34**, 2405962.
25. R. Elashnikov, O. Khrystonko, T. Jilková, S. Rimpelová, J. Prchal, I. Khalakhan, Z. Kolská, V. Švorčík and O. Lyutakov, *Adv. Funct. Mater.*, 2024, **34**, 2314420.
26. X. Ye, H. Huang, L. Chen, Y. Wang, M. Weng, L. Zhang and Z. Luo, *Chem. Eng. J.*, 2024, **483**, 149158.
27. N. Zhu, Q. Teng, Y. Xing, X. Wang, Z. Zhang and X. Wan, *Nano Lett.*, 2024, **24**, 12442-12451.
28. T. Cheng, Z.-T. Liu, J. Qu, C.-F. Meng, L.-J. He, L. Li, X.-L. Yang, Y.-J. Cao, K. Han, Y.-Z. Zhang and W.-Y. Lai, *Adv. Sci.*, 2024, **11**, 2403358.
29. R. Li, W. Jia, J. Wen, G. Hu, T. Tang, X. Li, L. Jiang, M. Li, H. Huang and G. Fang, *Adv. Funct. Mater.*, 2024, **34**, 2409207.